JOURNAL OF AIRCRAFT
Vol. 31, No. 2, March–April 1994

Drag Reduction of Airplane Fuselages Through Shaping by the Inverse Method

M. F. Zedan,* A. A. Seif,* and S. Al-Moufadi†
King Saud University, Riyadh 11421, Saudi Arabia

The axial singularity solution for the axisymmetric inverse problem has been extended to utilize doublet elements with linear intensity distribution. The solution converges faster than the source-based method, and is therefore quite promising. A procedure based on this solution has been used to design low-drag laminar fuselage shapes for small aircraft applications with a volumetric Reynolds number range of 10–30 million. A profile with a fineness ratio of 6, transition at 40% of body length, and volumetric drag coefficient of 0.012 at a nominal $R_\forall$ of 15 million, has been developed. The present inverse procedure was shown to be a powerful alternative to optimization methods. Several transition criteria were investigated in the course of the study. The Crabtree criterion appears to be the most consistent. Experimental transition data for axisymmetric bodies at high (flight) Reynolds numbers are urgently needed.

Nomenclature

$C_{D\forall}$ = volumetric drag coefficient based on $\forall^{2/3}$ as characteristic area
f_r = fineness ratio, body length/maximum diameter
H = boundary-layer shape factor, δ^*/θ
L = body length
l = length of an axial-singularity element
n = number of doublet elements
q = local velocity on body surface (at the edge of the boundary layer)
R_L = length Reynolds number based on U_∞ and L
R_s = Reynolds number based on local velocity and s
R_x = Reynolds number based on local velocity and x
R_θ = Reynolds number based on local velocity and θ
$R_\forall$ = volumetric Reynolds number based on U_∞ and $\forall^{1/3}$
r = local body radius and radial coordinate
s = length along body surface starting at nose
U_∞ = freestream velocity
u = axial component of q
v = radial component of q
X = nondimensional axial coordinate, x/L
X_{tr} = axial coordinate at transition
x = axial coordinate starting at nose
x_n = location of the starting point of singularity distribution along the axis
x_t = location of the end point of singularity distribution along the axis
$\forall$ = body volume
δ^* = boundary-layer displacement thickness
η = radial coordinate in element frame of reference
θ = boundary-layer momentum thickness
λ = pressure gradient parameter, $[-(\theta^2/\nu)(dq/ds)]$
μ = intensity of doublet distribution along axis
ν = kinematic viscosity
ξ, ζ = axial coordinates in element frame of reference
ψ = Stokes stream function

I. Introduction

PAST research in the area of maintaining natural laminar flow (NLF) on aircraft surfaces as a means of drag reduction has concentrated on wing design. The results of this relatively old research have recently been successfully implemented in the design of lifting surfaces of small aircraft. This was made possible by the advances in airplane construction techniques, resulting in smooth and accurate aerodynamic surfaces. Recently, Dodbele et al.[1] investigated the feasibility of designing laminar fuselage shapes for business aircraft. Their work was motivated by the fact that fuselage drag contribution is about 48% of the drag of an all-turbulent transport and up to 70% for a transport with laminar lifting surfaces.[2] Another motivation was the advent of new construction techniques producing surfaces of enough quality to maintain NLF at relatively high Reynolds numbers.[3] Using an optimization scheme, the authors were able to develop an axisymmetric body with $f_r = 6.14$ and $X_{tr} = 0.36$ for a fuselage of a business aircraft with $R_L = 40.86 \times 10^6$.

In optimization methods, the profile is represented by an expression consisting of a number of functions multiplied by unknown coefficients. These coefficients are determined by minimizing the drag coefficient subject to some constraints, such as a given fineness ratio, maximum velocity, etc. The choice of the forms of the shape functions is critical, otherwise the solution may converge to a profile that is not really the best in the absolute sense. This approach involves a large amount of calculations, and therefore, as stated by Slooff,[4] it "owes its existence entirely to the availability of large and fast computer systems." Slooff[4] further refers to it as "design by brute force" because of its black box nature. However, this approach is superior to other alternatives when one has to constrain certain parameters (e.g., fineness ratio, tail angle, etc.).

The objective of the present work is to use the axisymmetric inverse-design methodology[5] as an alternative to optimization methods, and to design laminar fuselage shapes for business and commuter aircraft. These inverse techniques are generally more effective than optimization schemes since they involve much less calculations and do not mask the physics of transition delay. In these methods, the body shape is determined for a given pressure distribution. By extending the region of favorable pressure gradient on the forebody, one can delay transition and consequently reduce viscous drag. Also, by reducing the pressure gradient on the aftbody, one can prevent separation, and therefore essentially eliminate pressure drag. This keeps physical insight in the design process. In principle, one can generate a body profile with specific characteristics, or at least judge the limits of drag reduction. In the course of the present study, the inverse method[6] has been

Received May 21, 1992; revision received Dec. 15, 1992; accepted for publication Dec. 15, 1992.

*Associate Professor, College of Engineering, P.O. Box 800.
†Currently Lecturer, King Faisal Air Academy, P.O. Box 2973, Riyadh 11461, Saudi Arabia.

improved by using axial line-doublet elements instead of line-source elements. Although doublets were used previously in the solution of the direct problem, this article appears to be the first to employ them in solving the inverse problem.

II. Practical Feasibility of Laminar Fuselages

The feasibility of maintaining appreciable runs of laminar boundary layer on modern production airplane surfaces over regions of favorable pressure gradients, has been demonstrated in recent flight tests by Runyan et al.[7] and Holmes et al.[8] The results of the latter study showed clearly that the laminar boundary layer is more persistent and durable on practical airplane surfaces produced by modern methods than previously expected. Transition downstream of the minimum pressure point was observed in many cases. Holmes et al.[3] showed that modern airframe construction materials and fabrication methods (composites, milled and bonded aluminum skins) produce surfaces with roughness and waviness better than critical values for the laminar flow at unit Reynolds numbers typical for high performance business airplanes.

Natural laminar flow has been a practical reality for sail planes with R_L from 4–7 × 10^6 (Refs. 3 and 9). Hertel,[10] as early as 1966, developed an axisymmetric fuselage shape characterized by small fineness ratio (f_r = 4.55), sharp nose, and rounded tail. It was shown that because of strong flow acceleration up to X = 0.4, the laminar boundary layer (LBL) can potentially survive up to X = 0.35 at R_L up to 100 × 10^6. Zedan and Dalton[11] predicted X_{tr} = 0.37 and C_{Dv} = 0.0114 for this body using the Crabtree criterion at R_v = 50 × 10^6 (R_L = 182 × 10^6). Carmichael[12] developed a laminar body characterized by an even lower fineness ratio (f_r = 3.33). The author tested a gravity powered model of this body (dubbed the Dolphin) in a low-turbulence ocean environment. X_{tr} was inferred to be between X = 0.45–0.58 for R_L = 20–40 × 10^6. Hanson and Hoyt[13] tested an axisymmetric body (f_r = 4.5) with a long run of favorable pressure gradient in a towing tank. By examining the velocity fluctuations in the boundary layer, the authors showed that the boundary layer stayed laminar up to the point of laminar separation near the minimum pressure point at R_v up to 3 × 10^6. Zedan and Dalton[5] used the inverse method with some success to modify this shape to reduce its drag coefficient. The limited success in this case indicates that the original shape is a near optimum shape. Zedan et al.[14] used the same inverse method to design a low-drag torpedo shape (f_r = 4.4) for R_v up to 20 × 10^6 (R_L = 75 × 10^6).

Aircraft fuselages are not exactly axisymmetric. Although the majority have circular cross sections, they do have a slightly cambered axis. Dodbele et al.[1] did their shape optimization work for an axisymmetric fuselage. The optimized shape was later fitted by the authors with the camber of an existing small aircraft. Goldschmied[15] also used an axisymmetric fuselage tested by NASA for the aerodynamic design of a small low-speed aircraft with a fuselage/wake propeller configuration.

III. Strategy for Fuselage Design by Inverse Method

To minimize the effort in determining the input to the inverse method, we start from the velocity distribution of a shape that has low drag in the Reynolds number range of interest. Two shapes are considered. The first is that of a modern low drag small aircraft[16,17] (f_r = 5.85), after removing its slight camber. The second is the shape developed by Dodbele et al.[1] with f_r = 6.14. Figure 1 indicates that these two shapes (dubbed here the "AV" and "DB" shapes, respectively) are quite similar. The drag characteristics of these two bodies and the fuselage shape of a typical commuter aircraft[16] are investigated in detail to gain insight in developing the velocity distribution required for inverse method input. The fuselage of the typical aircraft (dubbed "SB" in Fig. 1), which has long cylindrical midsection (f_r = 8.44), is used to provide a reference or baseline case for drag reduction. The volumetric Reynolds number calculated based on the range of cruising speeds and altitudes of these aircraft was found to be 10–25 × 10^6 for the AV fuselage, and 12–30 × 10^6 for the SB fuselage. After a careful evaluation of the transition characteristics of the low-drag fuselages, over a R_v range of 5–30 × 10^6, their velocity distribution is modified for the inverse method input with the objective of delaying transition. The drag characteristics of the bodies designed by the inverse method are also investigated in the same R_v range to show the improvement achieved over previous shapes.

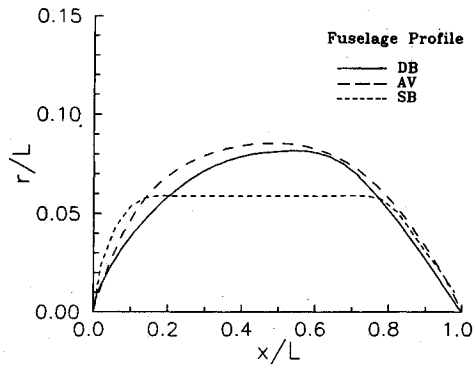

Fig. 1 Coordinates of the AV, DB, and SB fuselage shapes.

IV. Potential Flow Computational Techniques

The two most common approaches to solve potential flow around axisymmetric bodies are based on representing the body by a distribution of singularities, either along its axis or on its surface. The axial singularity approach is simpler and computationally much more efficient, while the surface singularity approach is more accurate for bodies with sudden changes in curvature and can handle nonaxisymmetric shapes. For the direct problem, Zedan and Dalton[6] showed that linear source elements along the body axis give velocity distributions with comparable accuracy to the surface singularity method[18] for most smooth body shapes in axial upstream flow. Kuhlman and Shu[19] showed that using linear axial source elements is more accurate than using linear doublet elements for axial flow. With the proper choice of the start and end of axial singularity distributions (X_n and X_t), their results were even more accurate than the surface singularity method, at a fraction of the computational cost. Hess[20] cautioned against these results because of the unsuitability of the test cases used. For bodies with sudden changes curvature, D'Sa and Dalton[21] showed that the surface singularity method is unquestionably more accurate. For solving the inverse problem, the methods based on axial and surface singularities are iterative. The surface singularity inverse method[22] typically converges in 10 iterations, while the axial source method[6] converges in four iterations with much less calculations per iteration.

Since low-drag shapes are generally very smooth, axial singularity methods are employed in the present work due to their computational efficiency and their reasonably accurate results for such shapes. In the following analysis, linear doublet elements are investigated as an alternative to linear source elements for solving both direct and inverse problems. The body is represented by n doublet elements along its axis as shown in Fig. 2. The stream function in the element coordinate system is given by

$$\psi(\xi, \eta) = -\int_0^l \frac{\mu_\zeta \eta^2 \, d\zeta}{[(\xi - \zeta)^2 + \eta^2]^{3/2}} \tag{1}$$

Similar expressions for velocity components u and v are obtained by the differentiation of Eq. (1). The intensity μ_ζ is assumed to vary linearly along the element according to

$$\mu_\zeta = \alpha + \beta\zeta \tag{2}$$

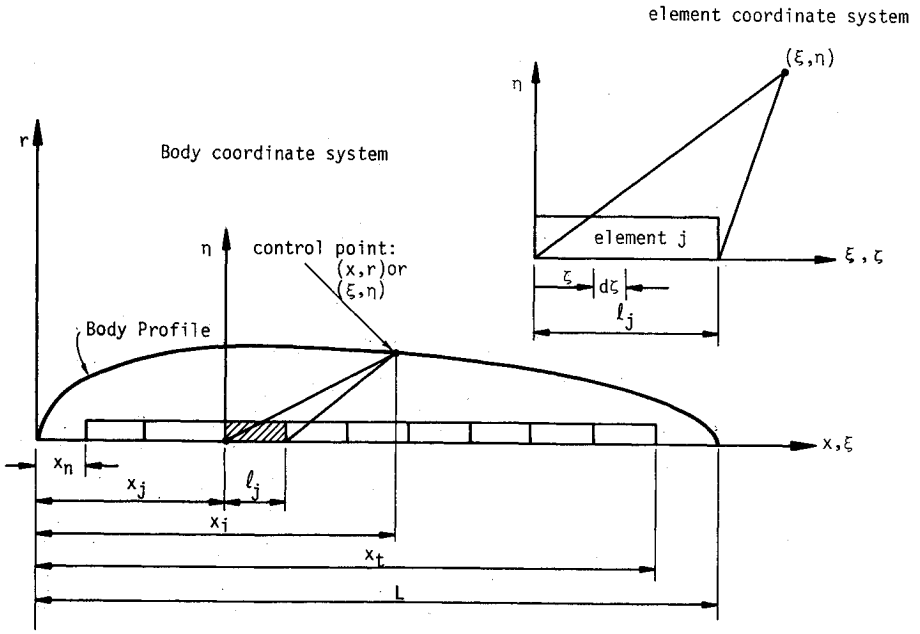

Fig. 2 Definition sketch of body and axial doublet elements.

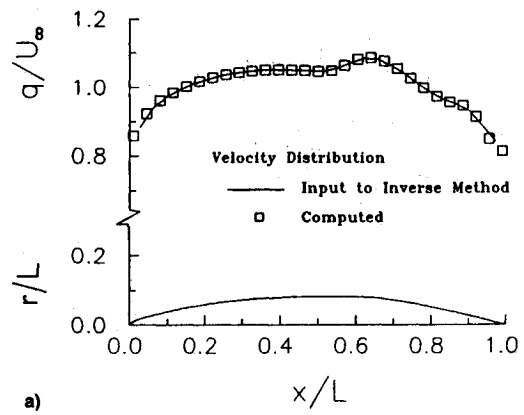

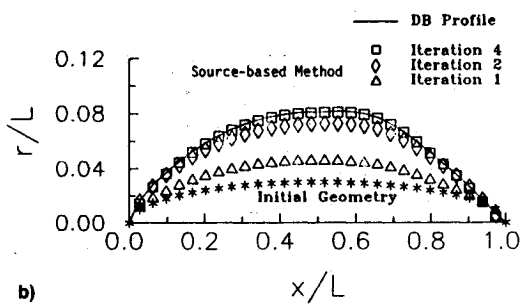

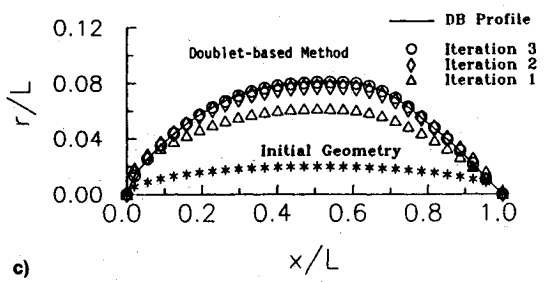

Fig. 3 DB profile and its a) velocity distribution, b) profile computed by source-based inverse method, and c) profile computed by doublet-based inverse method.

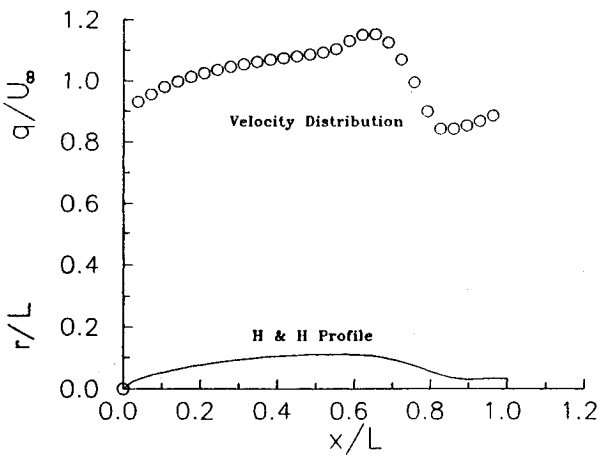

Fig. 4 Profile tested by Hanson and Hoyt[13] and its computed velocity distribution.

where α and β are constants to be determined from the conditions of continuity of μ at the nodes and $\psi = 0$ on the body surface. The number of these unknowns for a given body is $2n$; satisfying the continuity condition implicitly at the $(n - 1)$ nodes reduces the number of unknowns to $(n + 1)$. Adding the contributions of the elements and the freestream flow, and following a procedure similar to that of Zedan and Dalton,[23] expressions for ψ, u, and v at a control point i on the surface are derived. These expressions are represented by

$$\psi_i = \sum_{j=1}^{n+1} \bar{\psi}_{ij}\mu_{ij} + U_\infty \frac{r_i^2}{2} \tag{3}$$

$$u_i = \sum_{j=1}^{n+1} \bar{U}_{ij}\mu_j + U_\infty \tag{4}$$

$$v_i = \sum_{j=1}^{n+1} \bar{V}_{ij}\mu_j \tag{5}$$

where μ_j is the intensity at node j. Influence matrices ψ_{ij}, $\bar{U}_{ij}$, and $\bar{V}_{ij}$ are functions of body geometry only.

In the direct mode, μ_j are determined by applying Eq. (3) at $(n + 1)$ control points on body surface with $\psi_i = 0$, and solving the resulting $(n + 1)$ linear equations simultaneously.

Table 1 Summary of results of the H & H body

$10^{-6}\,R_v$	$X_{l.sep}$	C_{Dv} ($X_{tr} = X_{l.sep}$)	X_{tr} Michel-e^9	X_{tr} $H - R_x$	X_{tr} Granville	X_{tr} Crabtree	C_{Dv} ($X_{tr,crab}$)
0.5	0.677	0.0130	0.677	0.677	0.677	0.657	0.0138
0.7	0.677	0.0114	0.677	0.677	0.677	0.657	0.0122
1.0	0.677	0.0100	0.677	0.677	0.677	0.657	0.0108
1.5	0.677	0.0087	0.677	0.677	0.677	0.656	0.0094
2.0	0.677	0.0079	0.677	0.677	0.677	0.646	0.0091
3.0	0.677	0.0069	0.677	0.677	0.410	0.633	0.0086
4.0	0.677	0.0063	0.677	0.677	0.361	0.631	0.0080

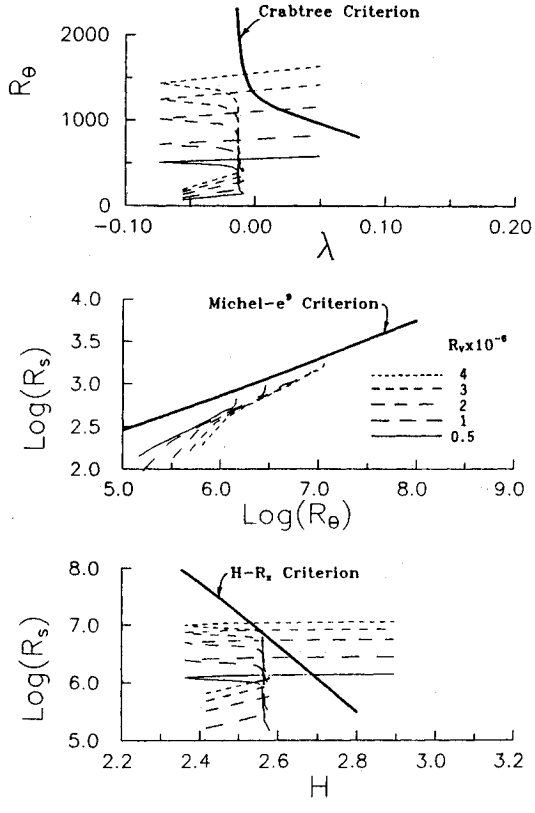

Fig. 5 Transition characteristics of the H & H body at different Reynolds numbers.

Substitution of μ_j into Eqs. (4) and (5) gives the velocity components at the control points. In the inverse mode, we use an iterative procedure starting from an assumed initial geometry. First u is calculated at the control points for this initial geometry from the given velocity distribution using the tangency condition

$$u_i = \frac{q_i}{\sqrt{1 + \left(\frac{dr}{dx}\right)_i^2}} \tag{6}$$

Then matrices $\bar{\psi}_{ij}$, $\bar{U}_{ij}$, and $\bar{V}_{ij}$ are also computed for the initial geometry. With u_i and $\bar{U}_{ij}$ known, Eq. (4) represents a system of $(n + 1)$ linear equations whose solution yields values for μ_j. Setting ψ_i to zero in Eq. (1), and with μ_j and $\bar{\psi}_{ij}$ known for the initial geometry, new values of r_i are determined. These values replace the initial geometry and the procedure is repeated until convergence is attained.

To verify the method, it was run for a low-drag shape with known solution. Figure 3a shows the body developed by Dodbele et al.[1] and its velocity distribution for axial upstream flow as computed by the present direct method. This distribution agrees well with the results of Dodbele et al.[1] Figures 3b and 3c show the body computed at different iterations by the source-based[6] and the present doublet-based inverse methods using this velocity distribution as input. The doublet-based method converges in three iterations compared to four iterations for the source-based method. The converged shape is almost identical to the exact profile in both cases. However, the doublet-based method appears to be quite sensitive to the choice of X_n and X_t, which are not known in advance. The above results were obtained with $X_n = 0.02$ and $X_t = 0.99$. The fast convergence of the method makes it worthwhile for further improvements.

V. Drag Package

The drag coefficient is calculated from the boundary-layer characteristics as the body tail is approached, using Young's formula.[24] Thwaite's integral method is used to compute the development of the LBL up to the point of laminar separation. An empirical transition criterion is used to find the location of transition along the body surface using the LBL solution. If no transition is indicated, transition location is assumed at the point of laminar separation. Patel's integral method[25] for thick boundary layers is used to compute the TBL development from the point of transition to the tail. Although these methods are somewhat old, the results of the package proved over many years to be as accurate as more sophisticated methods. For a known transition location, the predicted drag coefficient was in excellent agreement with measurements. For Gertler body 4165, tripped at $X = 0.05$, the present package gave $C_{Dv} = 0.0192$ at $R_L = 25.9 \times 10^6$, compared to a measured value of 0.0188; Parsons and Goodson[26] predicted 0.0203, and Dodbele et al.[1] predicted 0.0198 for the same body. Further verification of the package using a laminar profile with an extensive set of experimental results is presented later.

VI. Transition Criterion

This is the weakest link in the drag package. There seems to be the lack of a method that is reliable over a wide range of geometry and flow conditions. We tried the Michel-e^9,[27] $H - R_x$,[28] Crabtree,[29] and Granville[30] transition criteria on the low-drag body tested by Hanson and Hoyt.[13] This tail boomed low-fineness ratio body ($f_r = 4.5$) has an extended run of favorable pressure gradient (up to $X = 0.635$) as shown in Fig. 4. Signals from hot films flushly mounted on the body surface showed that transition occurred at, or just before, laminar separation for $R_v = 0.5$–4×10^6. Our laminar boundary-layer analysis gave laminar separation at $X = 0.677$; Hanson and Hoyt (H & H) calculated 0.68, while analysis by Dodbele et al.[1] gave 0.67. Figure 5 shows the computed LBL characteristics for this body at different Reynolds numbers plotted on the coordinates of the transition criteria of Crabtree, Michel-e^9, and the $H - R_x$. Table 1 shows X_{tr} obtained by different criteria, C_{Dv} computed using the X_{tr} predicted by the Crabtree criterion, and C_{Dv} computed with X_{tr} at laminar separation. No transition was indicated by the Michel-e^9 and the $H - R_x$ criteria before laminar separation at all Reynolds numbers. It should be noted that Michel-e^9 criterion is a combination of Michel's correlation and Smith and Gamberoni's

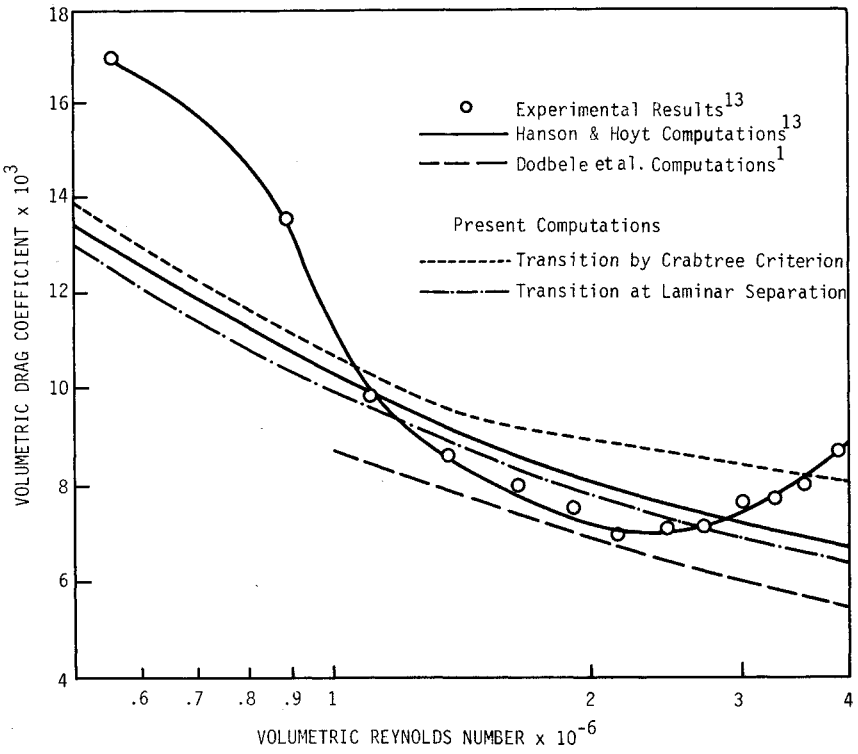

Fig. 6 Measured and computed drag coefficients of the H & H body at various Reynolds numbers.

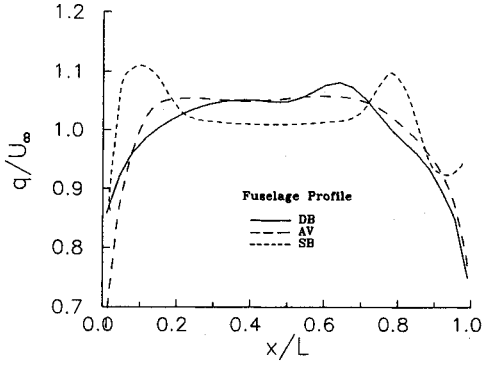

Fig. 7 Computed velocity distributions for the DB, AV, and SB fuselage profiles.

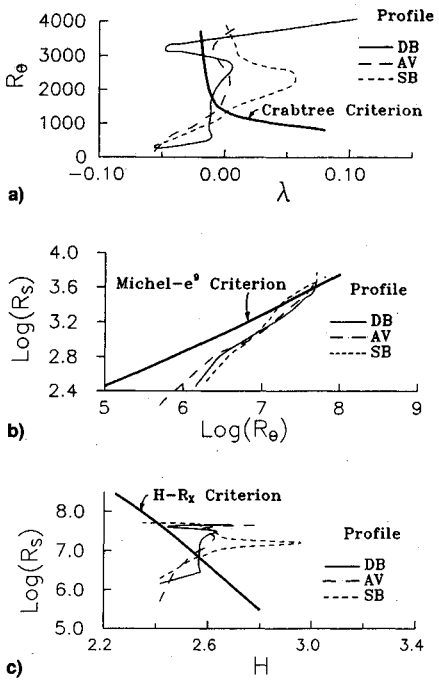

Fig. 8 Transition characteristics of the DB, AV, and SB profiles at a nominal R_V of 15 × 10⁶.

e^N correlation with $N = 9$. An expression for this combination was developed by Cebeci and Smith.[27] Granville criterion gave similar results up to $R_V = 2 \times 10^6$, after which X_{tr} drops sharply and unrealistically. The predictions of the Crabtree criterion indicate weak dependence of X_{tr} on R_V, giving X_{tr} slightly before laminar separation. The computed drag coefficients are plotted vs R_V in Fig. 6, together with the experimental results of Hanson and Hoyt.[13] Also shown in the figure are the computed results of H & H and Dodbele et al.,[1] both assuming transition at laminar separation. The corresponding present results lie in between and closer to the H & H curve. The present C_{DV} results, using Crabtree criterion for transition, are generally closer to experimental data at low Reynolds numbers and tend to somewhat follow the experimental trend at high Reynolds numbers.

VII. Results and Discussion

Assuming incompressible ideal flow at zero angle of attack, the velocity distributions on the conventional aircraft (SB), the low drag aircraft (AV), and the Dodbele et al.[28] (DB) axisymmetric fuselages are computed by the present direct method and shown in Fig. 7. It is no surprise that both the AV and the DB profiles have appreciable runs of accelerating flow in order to delay transition along the body surface. This is a common characteristic of low-drag profiles that will be greatly utilized in the inverse design. On the other hand, the SB profile has a small run of flow acceleration which is typical for turbulent bodies. The transition characteristics of these shapes at a nominal Reynolds number $R_V = 15 \times 10^6$ are shown in Fig. 8. The locations of transition for this and for other Reynolds numbers over the operating range of a small aircraft are shown in Fig. 9 for all shapes, as determined by different criteria. The results of the Crabtree criterion agree to some extent with those of the Granville criterion as extrapolated in the present study. Michel-e[9] consistently predicted X_{tr} substantially greater than other criteria, while the

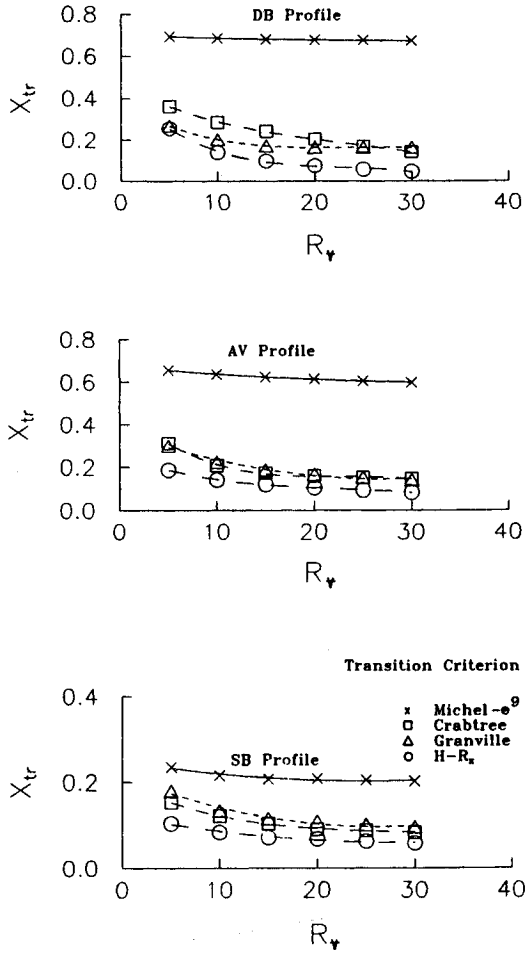

Fig. 9 Transition location obtained by different criteria as a function of Reynolds number for the DB, AV, and SB profiles.

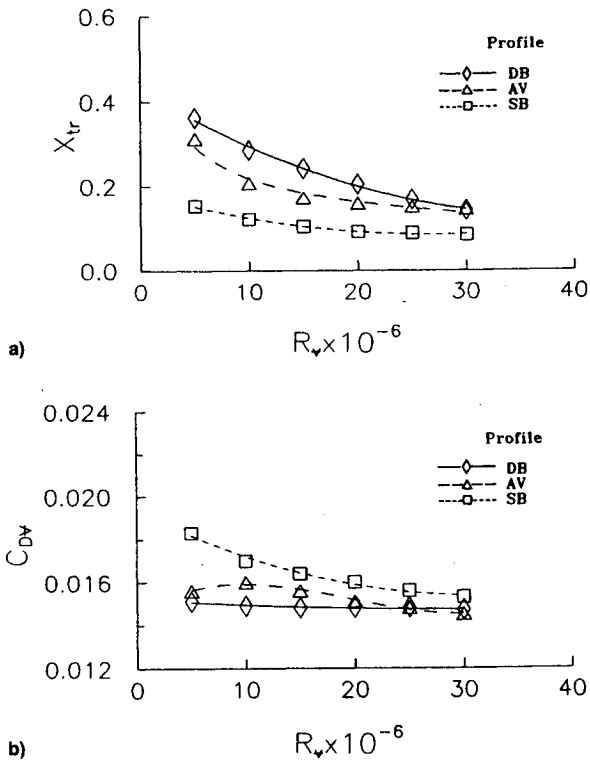

Fig. 10 Transition location predicted by a) Crabtree criterion X_{tr} and b) corresponding drag coefficient C_{DV} at various Reynolds numbers for the DB, AV, and SB profiles.

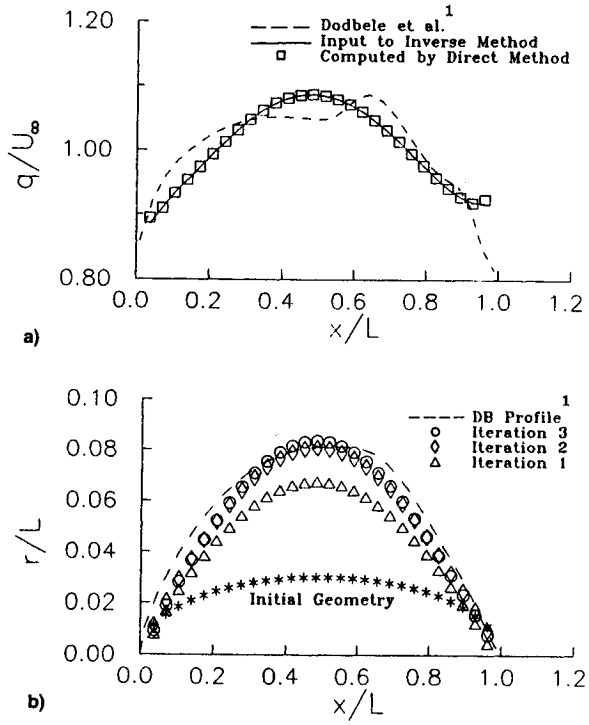

Fig. 11 a) Velocity distribution for inverse-method input and b) profile computed by the inverse method.

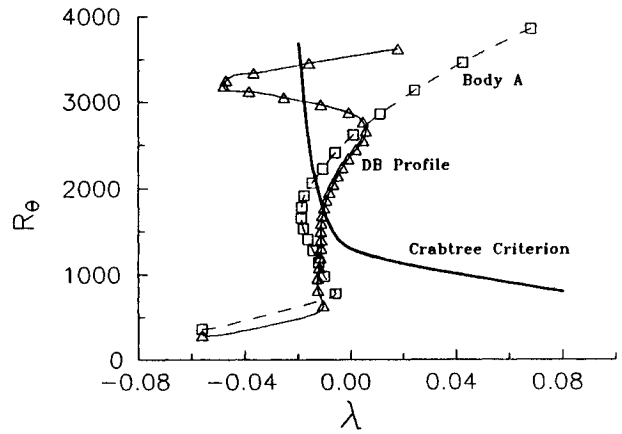

Fig. 12 Transition characteristics of the inversely designed body A and the DB profile at the nominal Reynolds number.

$H - R_x$ gave X_{tr} substantially smaller. Based on this and the results discussed earlier, it appears that the Crabtree criterion is the most consistent for the Reynolds number and body ranges under consideration. Figure 10a shows a comparison of X_{tr} predicted by the Crabtree criterion for the three shapes at different R_V, while Fig. 10b shows the corresponding C_{DV} results. Notice that in the present study, $\forall^{1/3}$ has been selected as a reference length in the Reynolds number, and $\forall^{2/3}$ selected as a reference area in the drag coefficient. The reason for this is that a fuselage is designed to provide volume,[31] and therefore, the objective would be to minimize drag for a given volume.

Since the DB profile performs best over most of the operating range, it provides the basis for the velocity distribution input to the inverse method. A careful examination of its transition characteristic at the nominal R_V in Fig. 8a shows that an increase in the favorable pressure gradient near the point where the characteristic crosses the Crabtree line ($X_{tr} = 0.242$; $R_\theta = 1741$, $\lambda = -0.0105$) would delay transition. After a limited number of successful trials, a number of in-

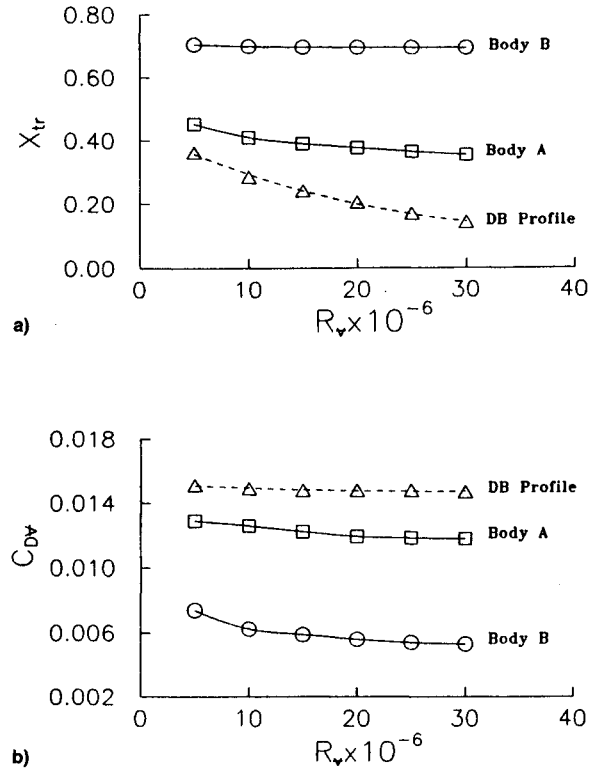

Fig. 13 Predicted a) transition location and b) corresponding drag coefficient for the inversely designed bodies A and B and the DB profile at various R_v over the operating range of a small aircraft.

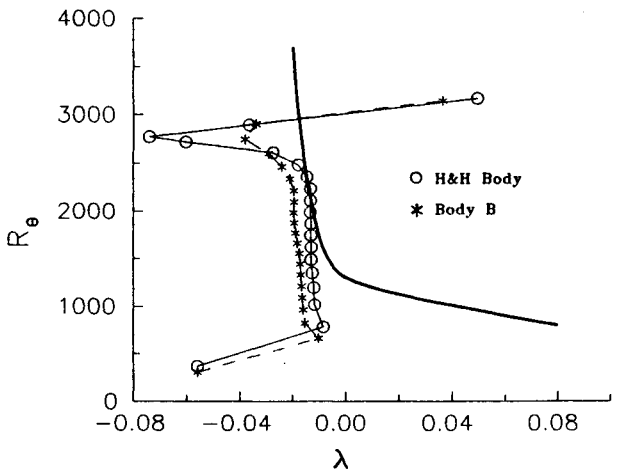

Fig. 14 Transition characteristics of the inversely-designed body B and the H & H body at the nominal Reynolds number.

versely designed shapes were obtained. Through these trials it became clear that the optimum shape depends on the design Reynolds number (as expected) and the transition criterion used. As R_v increases, the likelihood of early transition increases. To avoid early transition, the favorable pressure gradient along the forebody should be increased, thus making the input velocity distribution and the developed profile dependent on R_v.

To design a fuselage with f_r around that of the DB profile ($f_r = 6.14$), the maximum velocity has to be kept roughly the same. With this constraint, it appears that the best way to increase the flow acceleration near $X = 0.24$ is to move the velocity peak forward. This has the additional advantage of reducing the flow deceleration on the rear part of body, and therefore reducing the danger of separation. Figure 11a shows

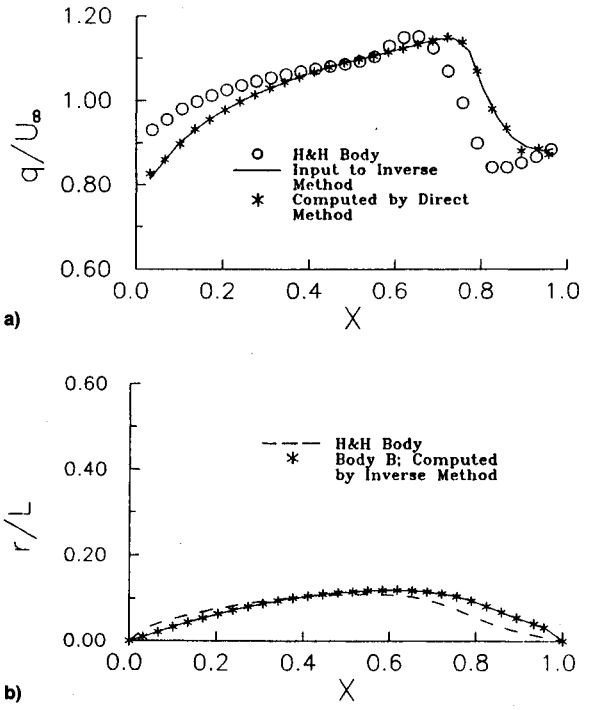

Fig. 15 Modification of the velocity distribution of the a) H & H body for inverse method input and the b) computed profile (body B).

a proposed velocity distribution together with the original DB velocity distribution; note that the maximum velocity ($q_{max}/U_\infty \cong 1.08$) has been moved forward from $X \cong 0.635$ to $X \cong 0.48$. The body computed by the inverse method at different iterations for this velocity distribution is shown in Fig. 11b. The converged shape (dubbed here as body A) has roughly the same f_r as the DB profile (around 6), but is less full near body ends with its maximum diameter at $X = 0.483$. The velocity computed for the designed shape by the direct method agrees very well with the suggested distribution as shown in Fig. 11a. The LBL transition characteristics of the DB profile and body A at design R_v (15×10^6) are shown in Fig. 12. The stabilizing effect of increasing the pressure gradient on the forebody on the laminar boundary-layer development is quite evident. The results show that transition has been delayed from $X_{tr} = 0.24$ to 0.39, while the TBL calculations indicated no turbulent separation up to $X = 0.99$. Its separation is indicated before that, the velocity distribution input to the inverse method is modified, and the whole design process is repeated. The computed drag coefficient drops as a result of this transition delay from 0.015 to 0.012. Boundary-layer and transition calculations were repeated at various Reynolds numbers covering the operating range: $R_v = 5\text{–}30 \times 10^6$, which corresponds to $R_L = 22.7\text{–}136 \times 10^6$. Figures 13a and 13b show transition locations and the corresponding drag coefficients for the two shapes. The improvement is evident over the whole range. Although the shape of a low-drag body is Reynolds number dependent in general, such effect is not felt in the present results because of the limited range of R_v. For instance, if R_v is much larger than present values, the boundary layer cannot be expected to stay laminar except for a smaller distance, and even for that small distance stronger flow acceleration is needed. The inverse method is handy in such cases where the velocity gradient (magnitude and length of run) can be varied in a convenient way to develop the appropriate shape.

So far, one body design has been presented. Other body designs with lower drag are possible if higher maximum velocity (lower fineness ratio) is acceptable. In that respect, the H & H body ($f_r = 4.5$) appears to provide a good starting profile (Fig. 4). The transition characteristic of this body at

the nominal R_v (15×10^6) barely crosses the Crabtree line at $R_\theta = 2080$, corresponding to $X = 0.37$ as shown in Fig. 14. This is considered to be a premature transition since a small correction in the velocity distribution near this location is all that is needed to prevent it. Other changes are also made in the velocity distribution in order to delay transition further and have a closed body as shown in Fig. 15. The body shape computed by the inverse method in iteration three (dubbed here as body B) which has $f_r = 4.15$, and maximum diameter at $X = 0.618$, and the H & H profile with faired tail[5] are also shown in this figure. Transition locations and corresponding drag coefficients for this body are included in Fig. 13. At the nominal R_v, we predict $X_{tr} = 0.7$ and $C_{Dv} = 0.0058$. While the drag performance of this body is superior to that of body A designed earlier, its fineness ratio is too low compared to current aircraft practice. This may present some limitation for aircraft designers in terms of aircraft stability and/or space utilization. Moreover, $X_{tr} = 0.7$ is not practically realistic when this shape is used for fuselage applications, because the wing-body junction[31] (likely to be at $X < 0.7$) is expected to trigger transition earlier. This profile, however, could be used for shaping external fuel tanks and stores.

VIII. Summary and Concluding Remarks

The inverse method based on axial singularities has been extended to utilize linear doublet elements instead of source elements. The method was shown to be a powerful alternative to calculation intensive optimization methods by applying it to the design of the axisymmetric fuselage of a small aircraft with an operating range of $R_v = 5\text{–}30 \times 10^6$. The transition characteristics of a low-drag modern aircraft fuselage, a conventional fuselage, a recently developed low-drag fuselage shape,[1] and another low-drag body with extensive and careful measurements[13] were studied in detail. Velocity distributions were developed based on this study for inverse method input. Two shapes with superior drag performance were obtained. One with $f_r = 6$, which is comparable to that of modern low drag fuselages, while the other body is thicker with $f_r = 3.9$. At a nominal R_v of 15×10^6, the computed transition locations for these two bodies are 0.39 and $0.7L$, and the corresponding volumetric drag coefficients are 0.012 and 0.0058, respectively. To our knowledge, these coefficients are lower than those reported in the literature for the same f_r and R_v. The profile with $f_r = 6$ superimposed on a slightly cambered axis appears to be a good candidate for shaping fuselages, while the thicker body is a candidate for shaping external fuel tanks and stores. Because of neglecting compressibility effects, these bodies are expected to perform better than calculated. Vijgen et al.[2] showed that density gradients in the LBL increase damping of Tollmien-Schlichting instability waves, and therefore, delay transition beyond incompressible calculations. The effects of deviation from axisymmetric shape on the LBL stability and transition need to be studied,[2] while the effects of wing-fuselage junction interference[31] are expected to be small if such a junction is at $X > X_{tr}$.

In the course of the study, different transition criteria were considered. For the operating R_v range of small aircraft, most of these criteria had to be extrapolated. The results were widely different in many instances. The most conservative was the $H - R_x$ criterion—always predicting very early transition, while Michel-e[9] was the most forgiving—yielding very late transition. The Crabtree criterion gave the most consistent results. Clearly, there is an urgent need for a reliable transition criterion, backed by experimental data at high (flight) Reynolds numbers, developed specifically for bodies of revolution. Wind-tunnel investigations are not suitable for this purpose because of their limited Reynolds numbers. Moreover, measuring the boundary-layer characteristics—and consequently, transition location and the drag for a body of revolution in a tunnel—is quite difficult because of vibrations, interference, and body support effects.

References

[1]Dodbele, S. S., Van Dam, C. P., Vijgen, P. M., and Holmes, B. J., "Shaping of Airplane Fuselages for Minimum Drag," *Journal of Aircraft*, Vol. 24, No. 5, 1987, pp. 298–304.

[2]Vijgen, P. M., Dodbele, S. S., Holmes, B. J., and Van Dam, C. P., "Effects of Compressibility on Design of Subsonic Fuselages for Natural Laminar Flow," *Journal of Aircraft*, Vol. 25, No. 9, 1988, pp. 776–782.

[3]Holmes, B. J., Obara, C., Martin, G. L., and Domack, C. S., "Manufacturing Tolerances for Natural Laminar Flow Airframe Surfaces," Society of Automotive Engineers Paper 850863, April 1985.

[4]Slooff, J., "A Study of Computational Methods for Subsonic and Transonic Aerodynamic Design," *Proceedings of the International Conference on Inverse Design Methods in Engineering Sciences*, (ICIDES), Univ. of Texas at Austin, Austin, TX, Oct. 1984, pp. 1–67.

[5]Zedan, M. F., and Dalton, C., "The Inverse Method Applied to a Body of Revolution with an Extended Favourable Pressure Gradient Forebody," *Communications in Applied Numerical Methods*, Vol. 2, Wiley, New York, 1986, pp. 113–119.

[6]Zedan, M. F., and Dalton, C., "Higher Order Axial Singularity Distributions for Potential Flow About Bodies of Revolution," *Computer Methods in Applied Mechanics and Engineering*, Vol. 21, No. 3, 1980, pp. 295–314.

[7]Runyan, J. L., Navran, B. H., and Rozendal, R. A., "F-111 Natural Laminar Flow Glove Flight Test Data Analysis and Boundary-Layer Stability Analysis," NASA CR-166051, Jan. 1984.

[8]Holmes, B. J., Obara, C. J., and Yip, L. P., "Natural Laminar Flow Experiments on Modern Airplane Surfaces," NASA TP-2256, June 1984.

[9]Althaus, D., "Wind-Tunnel Measurements on Bodies and Wing-Body Combinations," *Motorless Flight Research 1972*, NASA CR-2315, Nov. 1973.

[10]Hertel, H., "Full Integration of VTOL Power Plants in the Aircraft Fuselage," *Gas Turbines*, AGARD CP 9, Pt. 1, 1966, pp. 69–96.

[11]Zedan, M. F., and Dalton, C., "Viscous Drag Computation for Axisymmetric Bodies at High Reynolds Numbers," *Journal of Hydronautics*, Vol. 13, April 1979, pp. 52–60.

[12]Carmichael, B. H., "Underwater Drag Reduction Through Optimal Shape," *Underwater Missile Propulsion*, edited by L. Greiner, Compass Publications, Arlington, VA, 1966, p. 147.

[13]Hansen, R. J., and Hoyt, J. G., "Laminar to Turbulent Transition on a Body of Revolution with an Extended Favorable Pressure Gradient Forebody," *Journal of Fluids Engineering*, Vol. 106, June 1984, pp. 202–210.

[14]Zedan, M. F., Seif, A., and Hokail, Y., "The Modification of a Torpedo Shape by the Inverse Method for Reduced Drag," *Proceedings of the 2nd International Conference on Inverse Design Concepts and Optimization in Engineering Sciences*, Pennsylvania State Univ., University Park, PA, Oct. 1987, pp. 227–249.

[15]Goldschmied, F. R., "Aerodynamic Design of Low-Speed Aircraft with NASA Fuselage/Wake-Propeller Configuration," AIAA Paper 86-2693, Oct. 1986.

[16]Taylor, J. W. R. (ed.), *Jane's all the World's Aircraft 1988–89*, 79th Year of Issue, Janes Publishing, London, 1989, p. 164.

[17]McClellan, J., "Drag Eraser: The Piaggio P.180 Avanti Defeats Drag with an Arsenal of Curves, Fins and Flair," *Flying*, Vol. 116, No. 1, 1989, pp. 28–34.

[18]Hess, J., and Smith, A., "Calculation of Potential Flow About Arbitrary Bodies," *Progress in Aeronautical Sciences*, edited by D. Kucheman, Vol. 8, Pergamon, New York, 1966, pp. 1–138.

[19]Kuhlman, J. M., and Shu, J.-Y., "Potential Flow Past Axisymmetric Bodies at Angle of Attack," *Journal of Aircraft*, Vol. 21, No. 3, 1984, pp. 218–220.

[20]Hess, J. L., "The Unsuitability of Ellipsoids as Test Cases for Line-Source Methods," *Journal of Aircraft*, Vol. 22, No. 4, 1985, pp. 346, 347.

[21]D'sa, J. M., and Dalton, C., "Body of Revolution Comparisons for Axial- and Surface-Singularity Distributions," *Journal of Aircraft*, Vol. 23, No. 8, 1986, pp. 669–672.

[22]Bristow, D. R., "A Solution to the Inverse Problem for Incompressible Axisymmetric Potential Flow," AIAA Paper 74-520, June 1974.

[23]Zedan, M. F., and Dalton, C., "Potential Flow Around Axisymmetric Bodies: Direct and Inverse Problems," *AIAA Journal*, Vol. 16, No. 3, 1978, pp. 242–250.

[24]Young, A. D., "The Calculation of Total and Skin Friction Drags of Bodies of Revolution at Zero Incidence," ARC R&M 1874, April

1939.

[25]Patel, V. C., "A Simple Integral Method for the Calculation of Thick Axisymmetric Turbulent Boundary Layers," *Aeronautical Quarterly*, Vol. 25, Feb. 1974, pp. 47–58.

[26]Parsons, J. S., Goodson, R. E., and Goldchmied, F. R., "Shaping of Axisymmetric Bodies for Minimum Drag in Incompressible Flow," *Journal of Hydronautics*, Vol. 8, July 1974, pp. 100–107.

[27]Cebeci, T., and Bradshaw, P., *Momentum Transfer in Boundary Layers*, McGraw-Hill, New York, 1977.

[28]Dodbele, S. S., Van Dam, C. P., and Vijgen, P., "Design of Fuselage Shapes for Natural Laminar Flow," NASA CR-3970, March 1986.

[29]Crabtree, L. F., "Prediction of Transition in Boundary Layer of an Aerofoil," *Journal of the Royal Aeronautical Society*, Vol. 62, 1958, pp. 525–527.

[30]Granville, P. S., "The Prediction of Transition from Laminar to Turbulent Flow in Boundary Layers on Bodies of Revolution," *Tenth Symposium on Naval Hydrodynamics*, edited by R. D. Cooper and S. W. Doroff, U.S. Government Printing Office, Washington, DC, 1974, pp. 705–729.

[31]Wickens, R. H., "Aerodynamic Design of Low-Drag Fuselages," *Canadian Aeronautics and Space Journal*, Vol. 36, No. 4, 1990, pp. 189–201.